A Synchrotron SAXS Study of Structure Development Kinetics during the Reactive Processing of Flexible Polyurethane Foam

Michael J. Elwell, Stephen Mortimer, and Anthony J. Ryan*

Manchester Materials Science Centre, UMIST, Grosvenor Street, Manchester M1 7HS, United Kingdom

Received March 1, 1994®

ABSTRACT: The kinetics of microphase separation during the processing of flexible polyurethane foam have been investigated. Forced-adiabatic, time-resolved synchrotron SAXS experiments were employed to probe the evolution of structure. Microphase separation was observed to occur at a critical conversion of isocyanate functional groups and shown to follow the kinetics associated with spinodal decomposition. The isocyanate conversion at the microphase separation transition (MST) was in good agreement with our previously reported FT-IR results. From the scattering data, $R(q)$, the amplification rate of the composition fluctuations was determined. The data have been analyzed in terms of a time-dependent Ginzburg-Landau model (TDGL). Plots of $R(q)/q^2$ versus q^2 exhibited a maximum at a finite value of scattering vector (q). These observations were in qualitative agreement with the theoretical predictions of the TDGL theory.

Introduction

The reactive processing of water-blown flexible polyurethane foam from liquid monomers and oligomers involves a complex combination of both chemical and physical events. In less than 5 min, a liquid mixture of relatively low molecular weight components is transformed into the supramolecular architecture of solid foam. Information regarding both the reaction kinetics and development of morphology during processing is essential, such that an objective description of the events taking place and, ultimately, selective control of the process can be achieved.

Flexible polyurethane foam is formed by the simultaneous reaction of a diisocyanate with a polyether polyol and water. Combination of these two exothermic reactions leads to the formation of a segmented block copoly(urethane-urea), of the $-(H_mS)_n-$ type. This is blown into a foam by the cogeneration of carbon dioxide gas evolved from the water-isocyanate reaction. As the polymerization proceeds, the core of the rising foam bun becomes self-insulated by the surrounding polymer and this has the effect of bringing the process to occur under quasi-adiabatic conditions. Reaction kinetic studies during foam formation with both toluene diisocyanate (TDI) and methylene diphenyl diisocyanate (MDI) have been conducted previously and the results are documented in the literature.[1-5]

Analyses[6-8] of the final morphology present in flexible polyurethane foams employing small angle X-ray scattering (SAXS), dynamic mechanical spectroscopy (DMS), and differential scanning calorimetry (DSC) have shown them to exhibit a microphase-separated morphology similar to segmented urethane elastomers. The development of morphology during foaming is complex.[3,5] As the chemical reactions proceed, the chain lengths (N, degree of polymerization) of all the products increase and the interaction parameters (χ) can also change. Such changes can give rise to the system crossing thermodynamic boundaries which results in a transition from an initial homogeneous (disordered) state into a microphase-separated (ordered) state.[9,10] The resultant morphology is determined by the kinetic competition between polymerization and microphase separation.[7,9,10]

Scattering studies of the phase separation kinetics in multiblock copolymers are not common. To our knowledge there have been only five detailed reports published.[11-15] The first two pertain to styrene-butadiene-styrene triblock[11] and styrene-isoprene diblock systems,[12] respectively. The third by Ryan and co-workers[13] involved the study of the kinetics of phase separation by SAXS during the bulk polymerization of a copolyurethane. The hard segment was composed of MDI and butane-1,4-diol, and the soft segment was a poly(ethylene oxide), tipped poly(propylene oxide) diol of molar mass 2000 g/mol. The two remaining reports by Chu and co-workers[14,15] involved the study of the phase separation kinetics of copolyurethane samples which were quenched from the homogeneous melt phase to different annealing temperatures. The hard segments were composed of MDI and butane-1,4-diol.

The molecular connectivity in block copolymers restricts the spatial extent of the concentration fluctuations to dimensions of approximately twice the radius of gyration (R_g) of the entire block chain (≈200 Å). As a consequence, probing the phase separation kinetics calls for SAXS or SANS (small angle neutron scattering). In this paper we present results that have been obtained by employing the synchrotron SAXS technique to investigate the microphase separation behavior of water-blown flexible polyurethane foam, based on MDI and a polyether polyol, monitored under forced-adiabatic conditions. A comparison of the results obtained is made with our earlier results from forced-adiabatic, time-resolved FT-IR spectroscopy.[4] The scattering data are analyzed by a generalized time-dependent Ginzburg-Landau model of microphase separation kinetics proposed by Hashimoto[16] and previously employed by Connell and co-workers.[12]

Theory

Hashimoto[16] has proposed that the time variation of the order parameter, the difference between the average concentration in the homogeneous phase and the local concentration of the same component, in a block copolymer system which has undergone a quench to a lower temperature (or from a quench provided by an increase in χN) from an initially homogeneous state is given by a time-dependent Ginzburg-Landau theory. It has been shown[16] that the general form of the variation in scattered intensity $I(q,t)$, with time at fixed q following a quench is given by the following equation:

* To whom all correspondence should be addressed.
® Abstract published in *Advance ACS Abstracts*, August 15, 1994.

0024-9297/94/2227-5428$04.50/0

$$I(q,t) = I(q,0)\exp[2R(q)t] \quad (1)$$

The variation in $I(q)$ at a given time interval is determined by the scattering law, $P(q)$, in the homogeneous state. $R(q)$ is termed the growth rate constant and is given by eq 2, where M is the mobility term, G is the Gibbs free energy,

$$R(q) = -Mq^2\left[\frac{\partial^2 G}{\partial c^2} + 2kq^2\right] \quad (2)$$

and k is a gradient free-energy term. For the experiments that will be discussed here, the original derivation of Leibler[17] is most appropriate, i.e. the weak segregation limit. For an AB diblock copolymer with the average composition of the A block being ϕ_A, the final expression for $P(q)$ is given by

$$P(q) = \frac{N}{[F(x) - 2\chi N]} \quad (3)$$

where N is the degree of polymerization, χ is the Flory–Huggins interaction parameter between the component blocks, and $F(x)$ is an expansion in terms of the Debye function for the scattering from a single block copolymer molecule, and composition (in terms of volume fraction), where $x = q^2R_g^2$ and R_g is the radius of gyration of the whole block copolymer molecule.

At the spinodal point, eq 3 diverges (i.e. $-P(q)^{-1} = 0$) and is no longer a true description of the scattering at $\chi \geq \chi_s$ ($T \leq T_s$), where T_s is the spinodal temperature. The divergence and its variation with composition will define the phase boundary for the block copolymer. Modifications to eq 1 have been discussed previously by Cook[18] which take into account random thermal fluctuations (inclusion of a Brownian motion term). In employing eq 1 to analyze the data, the extremums are not strictly true. If $R(q)$ is positive, then at $t = \infty$, $I(q,\infty)$ is infinite; conversely, if $R(q)$ were negative, then the scattered intensity, $I(q,\infty)$, would be zero at infinite time following a quench. Furthermore, the q dependence of the Onsager coefficient, L_0, relating the diffusive flux of copolymer molecules to the local chemical potential has been neglected. This may be valid for the early stages of phase separation and a shallow quench. However, the latter point is not valid for the systems discussed here where there is a large thermodynamic quench. It should be noted the L_0 generally does have a q dependence. This dependence has been calculated by Pincus[19] for a polymer blend ($L_0 \propto q^{-2}$) but not for a block copolymer.

The important parameter in determining the position of the reaction mixture with respect to the phase boundary is the product χN. If the product $\chi N < (\chi N)_s$, then the value of $R(q)$ is negative. Neglecting the Onsager coefficient, L_0, $R(q)/q^2$ can be taken as a measure of the thermodynamic driving force for the growth of the concentration fluctuation with wave vector $q/2\pi$. A negative value indicates that such a concentration fluctuation will not grow but decay away. Thus, the system remains stable to concentration fluctuations of this particular wave vector. However, a different situation prevails if $(\chi N) > (\chi N)_s$. There is a region of q in which $R(q)$, and thus $R(q)/q^2$ are positive and the concentration fluctuations do not decay but grow and give rise to microphase separation. These growing concentration fluctuations have upper and lower critical boundaries to their wavenumbers. Outside these limits, the concentration fluctuations decay and do not contribute to the phase separation dynamics.[12] As originally published,[20] the Cahn–Hilliard theory of spinodal decomposition is a macroscopic description and has no direct relation to events at the molecular level.

Extensions to the theory have been made by de Gennes,[21] Pincus,[19] and Binder for polymer blends.[22] The thermodynamic driving force for the growth of the concentration fluctuation with wave vector $q/2\pi$, $R(q)/q^2$, becomes a maximum at $q = q_{max}$. Thus, the wavelength, $q/2\pi$, of the dominant Fourier component of the growing fluctuations in the early stages of phase separation is determined by the Fourier component that exhibits the maximum thermodynamic driving force. q_{max} is time independent in the early stages of phase separation and is controlled by thermodynamics. $R(q_{max})$ is further controlled by the transport properties.

$$D_{eff} = -\frac{2R(q)}{q_{max}^2} \quad (4)$$

The effective diffusion coefficient, D_{eff}, can be determined from the value of q where maximum scattering intensity occurs, q_{max}, during phase separation using eq 4. Binder[22] discusses equations that are identical in form to the Cahn–Hilliard equations, but they are couched in terms of the diffusion components of the homopolymer blend.

Experimental Section

To study the polymerization of flexible polyurethane foam via SAXS is difficult. The material undergoes an exotherm of 75–150 °C, the viscosity of the reaction medium increases from ≈10 to 10^4 Pa s, and the density decreases from 1000 kg m^{-3} to 30 kg m^{-3} in under 4 min. Translated into volume, this means that the final foam volume is some 33 times greater than the initial volume. Figure 1 shows typical experimental data for a flexible foam formulation prepared with 4.19 g of water/100.0 g of polyol. The reaction is highly exothermic, and the amount of material required to achieve self-insulation cannot be contained within a cell of the type previously employed by Ryan and co-workers[13] in an optical bench assembly on a synchrotron beamline. Ideally, the temperature of the SAXS sampling cell should be identical to that of the bulk foam throughout the reaction exotherm. If not, and the cell temperature is lower than that of the foam material in contact with the cell wall, the cell will effectively act as a heat sink and, as a consequence, will decrease the foam reaction exotherm, delay the reaction chemistry, and disrupt the resulting development of morphology. Thus, rapid heating of the cell is necessary in order to be able to replicate the reaction exotherm of the foam. Also, due to the rapid rate of the foaming reaction, it is necessary to employ reaction injection moulding (RIM) to meter, mix, and inject the reaction mixture into the cell. To circumvent the heat-loss problems, a new cell has been designed which can be positioned in the optical bench assembly of a beamline and fed with a reaction mixture from a micro-RIM machine.[13,23,24]

SAXS Cell. The temperature-controlled cell was constructed from aluminum and has an internal volume of ≈6.6 cm^3. It comprised two outer plates fitted with thermocouples and having countersunk holes of 4 mm diameter covered with polyimide (Kapton) windows of nominal thickness 10 μm. An aluminum insert of thickness 4.2 mm formed the "mold". The cross-sectional area of the mold is some 18 times that of the runner and gate assembly. The relatively high viscosity and the low flow rate provide for laminar flow of the material in the region of the windows. A top unit, which provided extra clamping capability to the two outer sections and the mold, was fitted with sockets such that the cylindrical heating elements could be fitted firmly in place. A Swagelock pipe was used so that the reaction mixture could be fed from the RIM machine nozzle via copper tubing (internal diameter of 1.68 mm and a typical length of 70 cm) to the SAXS cell mold. The cell itself was mounted on an X-Y translator for alignment in the X-ray beam. The cell was equipped with four, 250 W high-density cartridge heaters (Godfrey Thermal Limited, U.K.), one positioned at each corner of the cell. A small "chimney" of aluminum foil was fitted to the top piece of the cell

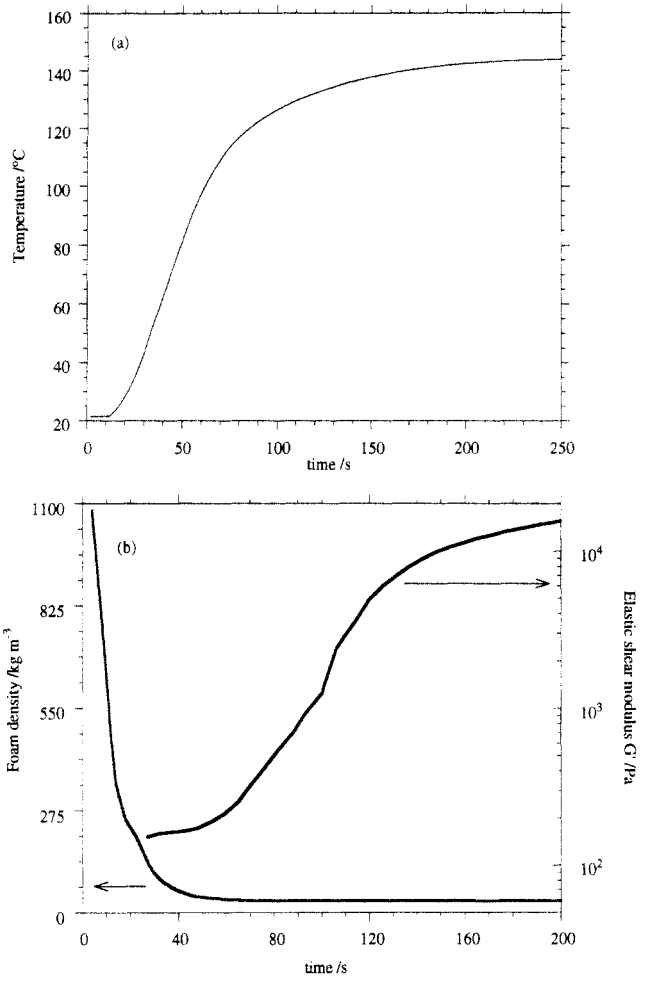

Figure 1. (a) Adiabatic temperature rise profile and (b) the rapid change in density and elastic shear modulus during the foaming reaction for the foaming system RIMSAXS-419.

to contain the excess foam and prevent the foaming mixture flowing over the top of the cell and making contact with the heating elements. A schematic diagram of the complete cell, equipped with foil chimney, cartridge heaters and type J thermocouples is given in Figure 2.

Temperature Control of the Cell. The temperature of the small angle X-ray scattering cell was controlled by a Macintosh II microcomputer equipped with Strawberry Tree Incorporated Workbench V3.1 system software and ACM2-12-8 (T51) data acquisition A-D hardware. The adiabatic temperature rise profile was prerecorded and played back as the set-point on a PID controller. Further details are documented elsewhere.[5]

Materials. Model flexible foam formulations with water concentrations of 2.10 and 4.19 g/100.0 g of polyol were employed throughout the work. Details of the formulations are provided in Table 1. In all the discussions that follow, the formulation containing 2.10 g of water/100.0 g of polyol will be referred to as RIMSAXS-210 and that containing 4.19 g of water, RIMSAXS-419.

Micro-RIM Machine. In order to be able to meter, mix, and inject a reactant stream into the cell such that accurate control of stoichiometry was maintained, a micro-RIM machine was employed. The machine has been designed to be portable to interface with analytical instruments[23,24] and is of such a size that it could be brought into the experimental hutch without difficulty.

Synchrotron SAXS. SAXS measurements were made on beamline 8.2 at the Synchrotron Radiation Source (SRS) at the SERC Daresbury laboratory, Warrington, U.K. With the SRS operating at 2 GeV and 200 mA, a flux of 4×10^{10} photons s^{-1} is generated at the sample position. A vacuum chamber is positioned between the sample and detector in order to reduce air scattering and absorption. Both the exit window of the beamline and the entrance window of the vacuum chamber are made from 15 μm mica; the exit window of the vacuum chamber is made from 10 μm Kapton. A beamstop is mounted just before the exit window to prevent the direct beam from hitting the detector. The camera is equipped with a multiwire quadrant detector. The quadrant detector has an opening angle of 70° and an active length of 0.2 m. This detector measures intensity in the radial direction. It has an advantage over single wire detectors in that the active area increases radially. The detector can handle count rates up to approximately 250 000 counts s^{-1}. For the calibration of the sample to detector distance, the scattering pattern from an oriented specimen of wet collagen (rat-tail tendon) was used. Parallel plate ionization counters were positioned before and after the SAXS cell and recorded the incident and transmitted intensities. Thus, changes in the attenuation factor of the specimen (transmission and thickness) resulting from the density changes during the foaming process could be monitored continuously. The experimental data obtained were corrected for background scattering (subtraction of the scattering from the empty cell and camera), sample thickness and transmission, and the positional alinearity of the detector. A schematic diagram that shows the complete experimental arrangement that was employed is illustrated in Figure 3. The SAXS patterns were recorded every 2 s. The temperature of both the cell and the reacting foam were recorded at a frequency of 1 Hz over a period of 512 s. For each run, the shot volume was typically 12.5 cm^3 and the shot time was 0.42 s. The material at the window was approximately 0.05 s old. Finally, a 5 mm cube section of foam was removed from the chimney section after 30 min and a static SAXS pattern of the "final morphology" was obtained.

Results

Temperature Control of the Cell. A comparison of the temperature profiles for the reference temperature, the thermal response of the cell, and the foam within the cell are illustrated in Figure 4 for both RIMSAXS-210 and RIMSAXS-419 foaming systems. For RIMSAXS-210 there is an initial short delay in the response of the cell of approximately 5–10 s. This results from the finite time required for relaying the signal around the circuit and the initial response of the heating elements. In the case of RIMSAXS-419, this initial delay is approximately 5 s longer. RIMSAXS-419 has a greater thermal lag than RIMSAXS-210 because its increased water concentration results in a more rapid rate of temperature rise. This demands a much faster response from the heating elements within the cell. What is important is that the cell does not act as a heat sink for the foam within the cell. The difference in temperature between the reference and the cell will clearly have an effect on the value of the isocyanate conversion determined. The error in the isocyanate conversion resulting from the difference in temperature between the reference and the cell is shown in the inset caption of Figure 4.[5] The upper curve represents RIMSAXS-419 and the lower curve, RIMSAXS-210. T_{ref} is the reference temperature at time t and T_{cell} is the temperature of the cell at any time t. The error in the isocyanate conversion at the onset of microphase separation ($t = 120 \pm 2$ s) and the physical gel point ($t \approx 180$ s) is within 1% for RIMSAXS-210. In the case of RIMSAXS-419, the maximum error in p_{NCO} is approximately 5% at the onset of microphase separation ($t = 60 \pm 2$ s) and the error reduces to approximately 1% at physical gelation ($t = 80 \pm 2$ s).

Correlation between the Foam Density Calculated from Volume Rise Profiles and That Calculated from the Intensity of the Rear Ionization Counter. Parallel plate ionization counters were positioned before and after the SAXS cell, and these recorded the incident and transmitted intensities. This allowed changes in the attenuation factor of the specimen (transmission and

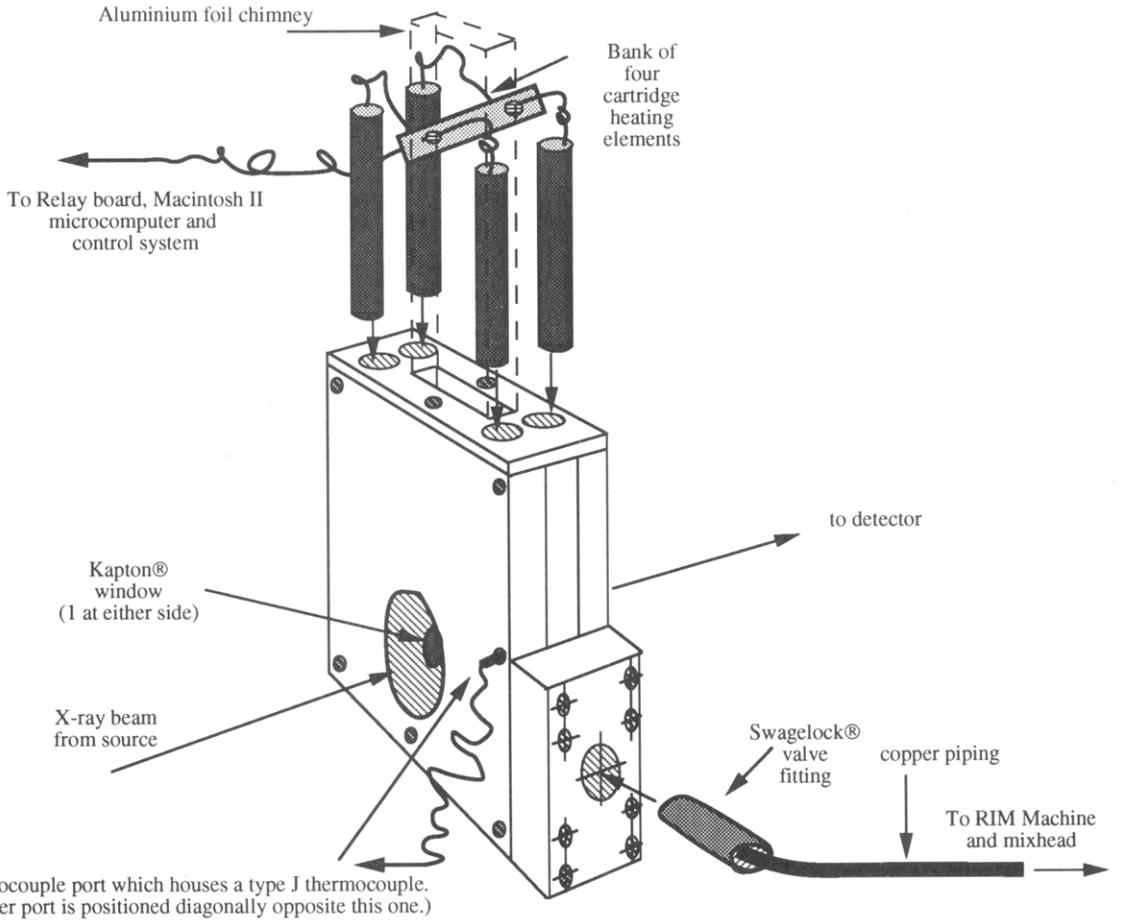

Figure 2. 3-D schematic diagram of the SAXS sampling cell.

Table 1. Details of the Foam Formulation Components

formulation component	foaming system RIMSAXS-210 mass/g	RIMSAXS-419 mass/g
polyether polyol	100.00	100.00
isocyanate	37.10	67.66
distilled water	2.10	4.19
tertiary amine catalyst	0.70	1.80
silicone surfactant	4.00	4.00

thickness) resulting from the change in sample density during the foaming process to be monitored continuously. Figure 5 is a plot of the intensity from the rear ionization counter response during the reaction for a typical data set obtained from RIMSAXS-210. The change in foam density was calculated by normalization of the intensity change exponentially (since intensity is proportional to $e^{-\rho}$). This was then scaled with the initial density of the reaction mixture. Reasonable agreement between the density calculated as a function of time from the absorption of the X-rays and that from foam volume expansion profiles measured by ultrasonic methods[4,5] was observed. In addition, the final foam density observed in the SAXS experiments was in close agreement with that obtained from laboratory bench-scale foaming. Figure 6 compares the density change observed from the volume rise profiles with that determined from the absorption of the X-rays.

Synchrotron Small X-ray Scattering. Representative time-resolved SAXS data that have been collected during foam formation are presented in Figures 7 and 8 for RIMSAXS-210 and RIMSAXS-419, respectively. They are three-dimensional plots of intensity $I(q,t)$, versus scattering vector, q, versus time, t. The first frame (an empty cell) has been subtracted from the subsequent patterns to remove the background (cell and camera) scattering. The data have also been corrected for changes in transmission (due to the density change) and the positional alinearity of the detector. It will be observed that for both systems, there is an initial upturn in $I(q)$ at low q. It is proposed that this is due to the filling of the cell with a liquid that contains air bubbles which are growing in size. The air bubbles are of approximately 1–10 μm in diameter at the start of the reaction. It is thermodynamically more favorable for the carbon dioxide which is evolved from the water–isocyanate reaction to undergo diffusion into the existing bubbles than to undergo self-nucleation to evolve a new bubble under the conditions of foam formation.[25] It should be emphasized that the number of bubbles remains approximately constant.[25] The air bubbles (which are introduced by mechanical agitation prior to loading of the polyol blend into the tank of the RIM machine) act as the nucleation sites and grow due to the diffusion of carbon dioxide from the water–isocyanate reaction. At the end of the reaction, the mean cell diameter is on the order of 200–600 μm.

The patterns for both systems illustrate that in the early stage of the reaction, there is a homogeneous liquid present. In the case of RIMSAXS-210, after 120 ± 2 s (see Figure 12a), there is the first appearance of a scattering maxima and this occurs at $q \approx 0.06$ Å^{-1}. The intensity at this scattering maxima continuously increases until approximately 200 s, after which, the growth in the peak intensity slows down. Beyond 220 s, the peak intensity becomes approximately constant. This is after the expanding foam has reached the Berghmans point[26] (onset of vitrification, $p_{NCO} = 0.71 \pm 0.02$). In the case of RIMSAXS-419, after

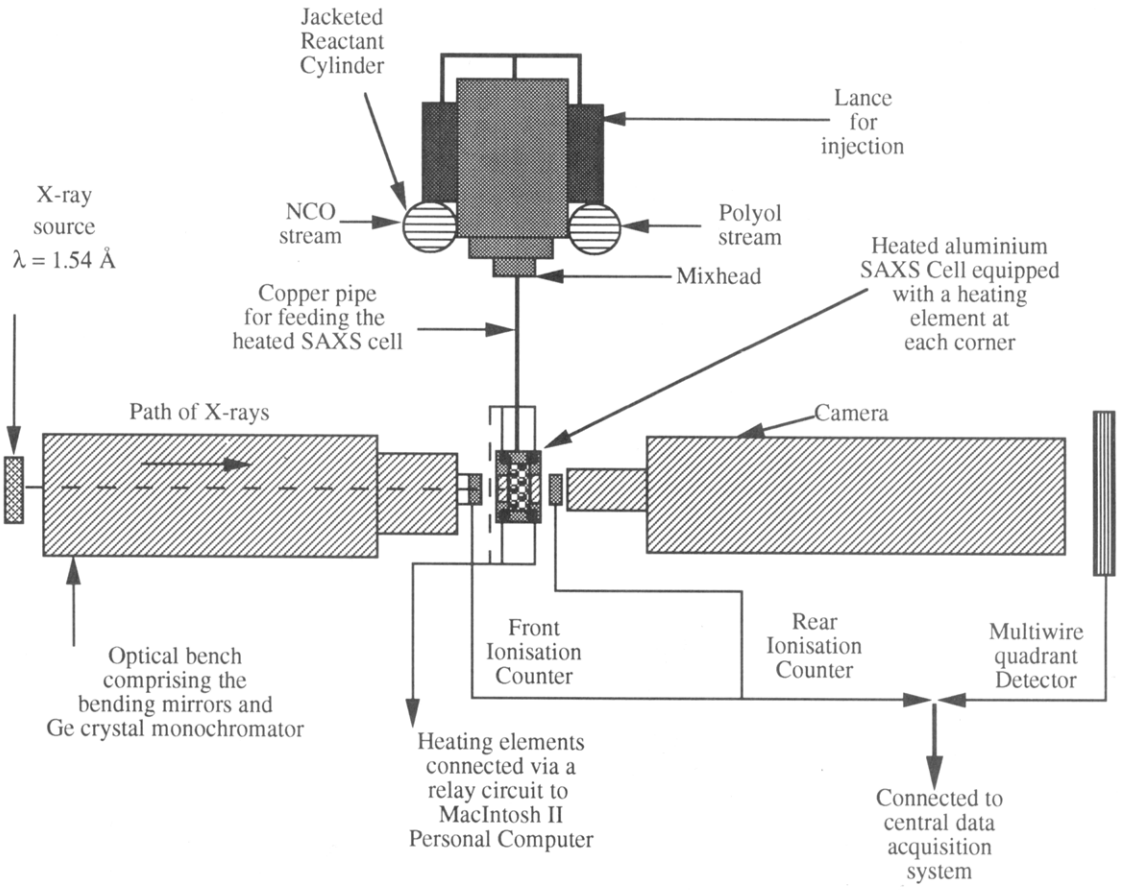

Figure 3. Schematic diagram illustrating the complete experimental arrangement within the X-ray hutch.

60 ± 2 s (refer to Figure 12b), there is the first appearance of a scattering maxima and this occurs at $q \approx 0.05$ Å^{-1}. The intensity at this scattering maxima continuously increases until approximately 80 ± 2 s, after which the growth of the peak intensity slows down. Beyond 96 ± 2 s, the peak intensity becomes approximately constant. As with RIMSAXS-210, this is after the vitrification (p_{NCO} = 0.71 ± 0.02) of the expanding foam. The longer induction time prior to the appearance of the scattering maxima in RIMSAXS-210 results from the lower rate of reaction of this system compared with that of the higher water concentration system, RIMSAXS-419. Such observations were reproducible on a run to run basis (×5 runs) for the two systems investigated.

Interdomain Spacing. The maximum in $I(q)$ suggests the presence of structure with periodic electron density within the sample. The most common practice for determining the periodicity is to report the Bragg spacing, d, as given by eq 5. Figure 9 is a plot of $I(q)$ versus q at

$$d = 2\pi/q_{max} \tag{5}$$

selected times, for a representative data set for the foaming system RIMSAXS-419. The maximum in $I(q)$ occurs at $q \approx 0.05$ Å^{-1}, yielding an interdomain spacing of 126 Å. This was reproducible to within ±2 Å on a run to run basis. For the foaming system, RIMSAXS-210, the interdomain spacing was calculated to be 105 Å. This was reproducible on a run to run basis to within ±3 Å. The d spacing did not change during the structuring process for either system.

Degree of Microphase Separation. The growth in scattered intensity during the polymerization can be related to the degree of microphase separation through the square of the electron density variance, $\langle \eta^2_0 \rangle$. The ideal electron density variance, $\langle \eta^2_0 \rangle$ (electrons^2 cm^{-6}), of a perfectly separated two-phase system with sharp phase boundaries is given by eq 6. Where η is the average electron

$$\langle \eta^2_0 \rangle = \phi_1^0(\eta - \eta_1^0)^2 + \phi_2^0(\eta - \eta_2^0)^2 \tag{6}$$

density of the material, and ϕ^0 and η^0 are the volume fraction and electron density of the two pure phases, respectively. A real system will contain thermal density fluctuations and diffuse boundaries between the phases. In this case, the actual electron densities are closer to the average, leading to a decrease in the electron density variance of the real system which is given by eq 7. The

$$\langle \eta^2 \rangle = \phi_1(\eta - \eta_1)^2 + \phi_2(\eta - \eta_2)^2 \tag{7}$$

value of $\langle \eta^2 \rangle$ will thus vary between zero for a homogeneous mixture and $\langle \eta^2_0 \rangle$ for a fully microphase-separated block copolymer. Experimentally, the electron density variance may be calculated from eq 8. Where i_e is the Thompson

$$\phi(1 - \phi)\langle \eta^2 \rangle = Q/2\pi i_e = \int_0^\infty I(q) q^2 \, dq \tag{8}$$

scattering factor and the quantity Q is known as the invariant. It is known as the invariant because it is independent of the size or spatial arrangement of structural heterogeneities. The invariant is a linear function of the electron density variance, $\langle \eta^2 \rangle$, and a quadratic function of the volume fraction, ϕ. The experimental invariant can be employed to characterize the structural development as well as the degree of microphase separation. Determination of the electron density variance, $\langle \eta^2 \rangle$, requires absolute invariant data which in turn require absolute intensity measurements. The absolute intensity

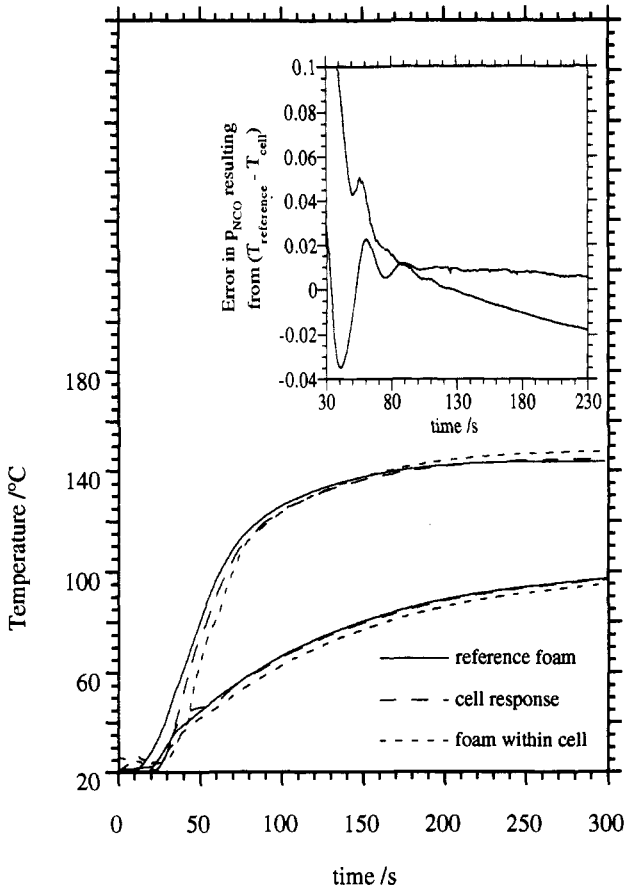

Figure 4. Comparison of the temperature profiles for the reference driver file, the cell response, and the foam within the cell for RIMSAXS-210 (lower curves) and RIMSAXS-419 (upper curves). The inset shows the error in the isocyanate conversion resulting from the difference in temperature between the reference and the cell.

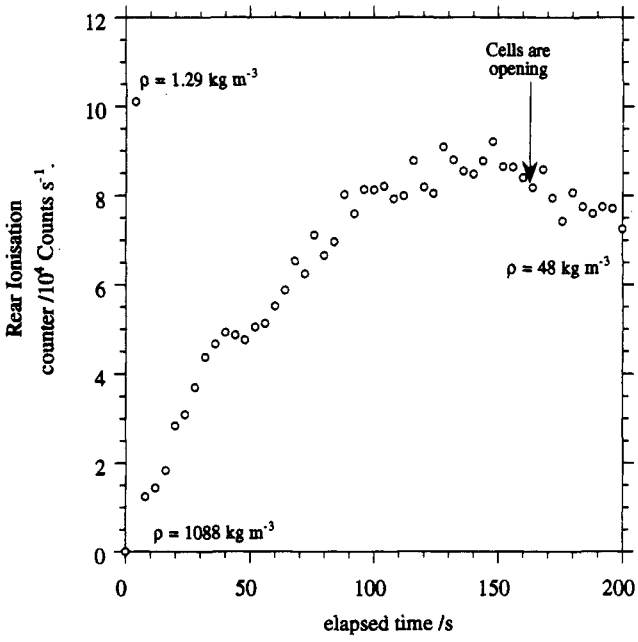

Figure 5. Intensity from the rear ionization counter as a function of elapsed time for a representative data set, obtained from the foaming system RIMSAXS-210.

requirement is not readily feasible on SAXS cameras that have pseudo-pin-hole optics.[27] Calculation of the absolute invariant also requires subtraction of the thermal background, extrapolation from $q = 0$ to the first data point, and extrapolation from the last data point to $q = \infty$.

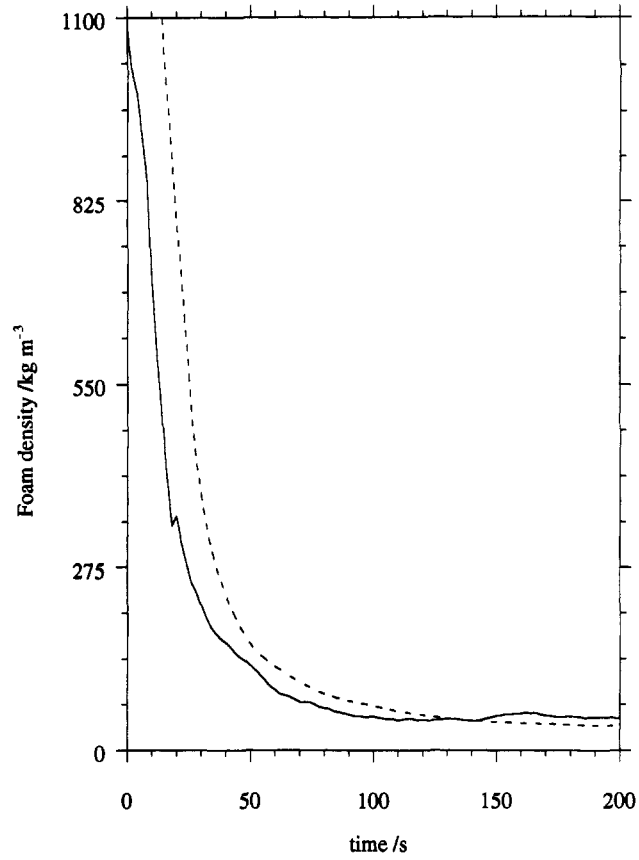

Figure 6. Comparison between the change in foam density observed from the volume rise profile (broken line) with that determined from the absorption of the X-rays (solid line) for the foaming system RIMSAXS-210.

The relative invariant, Q', in eq 9, has been calculated by summation of the area under the $I(q)q^2$ versus q curve between the first reliable data point ($q_1 = 0.02$ Å^{-1}) and the region inwhich $I(q)q^2$ becomes constant ($q_2 = 0.12$ Å^{-1}).

$$Q' = \int_{q_1}^{q_2} I(q)q^2 \, dq \tag{9}$$

Figure 10 is a plot of the relative invariant, Q', versus time. It is proposed that the initial behavior of Q' is related to the contrast between the bubbles and the reacting liquid. After 60 s the invariant is dominated by the contrast between the microphases in the polymer. The following argument is put forward in support of this hypothesis.

It is assumed that the overall electron density variance comprises two additive contributions, viz. that from the electron density difference between the hard- and soft-segment phases and that from the electron density difference between the liquid reactant and the gas (CO_2) within the bubbles. This can be described by the following equation:

$$\langle \eta^2 \rangle = \{\phi_{HS}(1 - \phi_{HS})(\eta_{HS} - \eta_{SS})^2\} + \{\phi_b(1 - \phi_b)(\eta_1 - \eta_b)^2\} \tag{10}$$

where $\langle \eta^2 \rangle$ is the overall electron density variance, ϕ_{HS} is the volume fraction of hard segment, η_{HS} is the electron density of the hard-segment phase, η_{SS} is the electron density of the soft-segment phase, ϕ_b is the volume fraction of bubbles, η_1 is the electron density of the homogeneous liquid, and η_b is the electron density of the gas within the bubble film.

Considering only the initial 50 s (since between this point and the MST, the relative invariant, Q', is small) if the contribution from bubble/liquid scattering is the

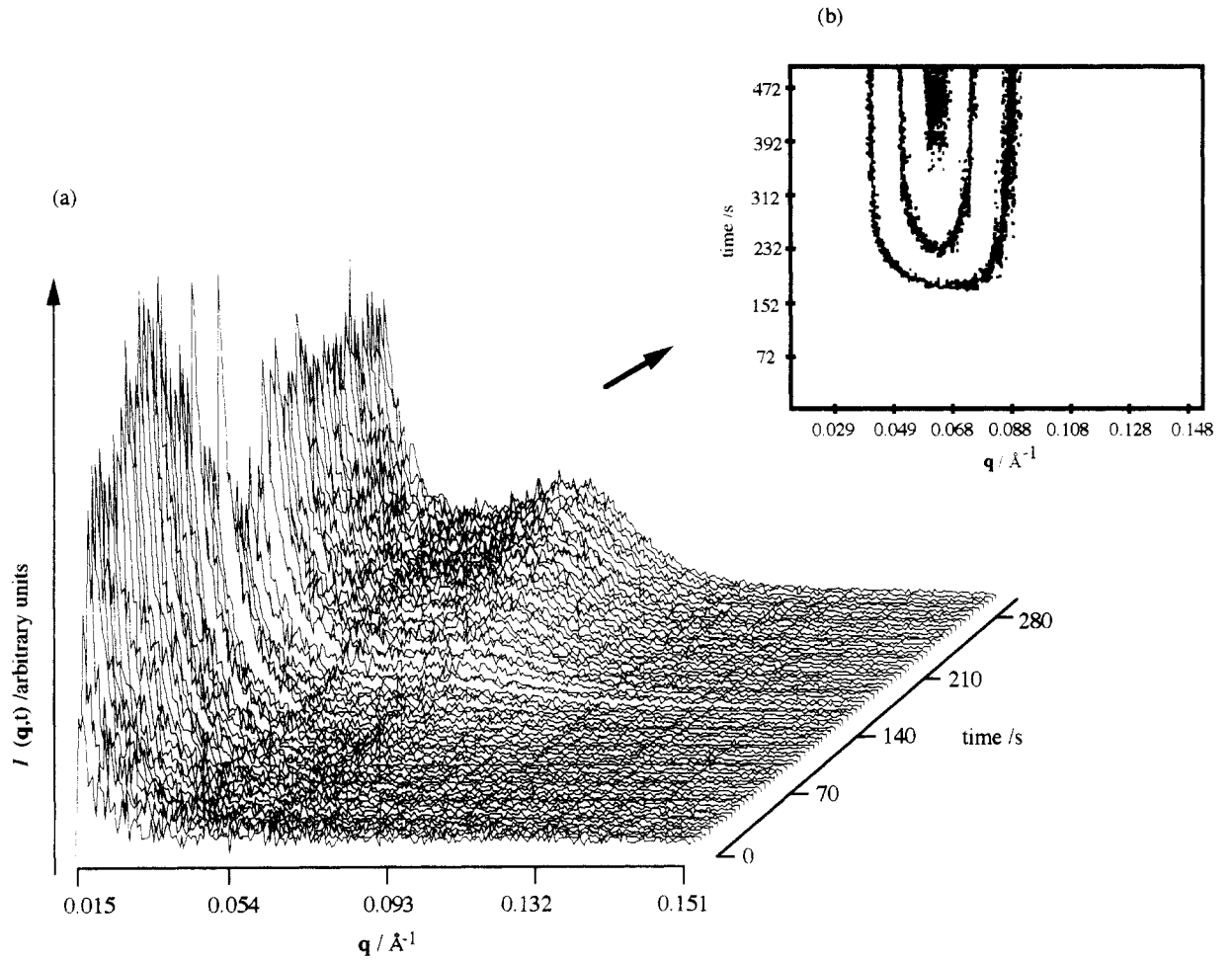

Figure 7. (a) Three-dimensional plot of scattered intensity $I(q,t)$, versus scattering vector, q, versus reaction time, t, for a representative data set for the foaming system RIMSAXS-210. (b) Two-dimensional contour plot of time, t, versus scattering vector, q, for the 3-D data illustrated.

dominant term in eq 10, then to a first approximation the electron density variance of the liquid mixture, $\langle \eta^2 \rangle$ is given by eq 11. Since the scattering intensity obtained is

$$\langle \eta^2 \rangle \approx \phi_b(1 - \phi_b)(\eta_1 - \eta_b)^2 \tag{11}$$

relative, then neglecting the constants, the relative invariant, Q', to a first approximation is given by eq 12. ϕ_b is known as a function of reaction time. A value for $(\eta_1 - \eta_b)^2$

$$Q' \approx \phi_b(1 - \phi_b)(\eta_1 - \eta_b)^2 \tag{12}$$

can be calculated at a specific time because Q' is known as a function of time experimentally. Assuming that $(\eta_1 - \eta_b)^2$ remains approximately constant (given by C_1), eq 12 can be approximated to eq 13. Figure 11 is a comparison

$$Q' \approx \phi_b(1 - \phi_b)C_1 \tag{13}$$

between $Q'(t)$ predicted using eq 13 and the measured density and $Q'(t)$ observed from experiment. It will be observed from Figure 11 that there is close agreement between the two sets of data, particularly in the initial period of the reaction. Any difference is due to the value of C_1, and this becomes more pronounced between the predicted and observed values at around 30 s. At this time there is little change in the volume fraction of the bubbles and thus the contribution from the liquid/bubble scattering is approximately constant. Since the predicted values continue to decrease, there is a change in the electron density difference with time (temperature) between the liquid and the gas, $(\eta_1 - \eta_b)^2$, that the approximation does not take into account. Although the agreement between the predicted and observed value breaks down after approximately 30 s, the hypothesis that the maximum in the relative invariant early in the reaction is due to $\phi_b \approx 0.5$, and the changes in relative invariant early in the reaction arise from the contribution of liquid/bubble scattering would appear to be a valid one.

From Figure 10, the onset of microphase separation is taken as 60 ± 2 s. This corresponds to an isocyanate conversion, $p_{NCO} = 0.54 \pm 0.02$. For multiple runs on both RIMSAXS-210 and RIMSAXS-419, it was observed that the onset of microphase separation occurred at $p_{NCO} = 0.54 \pm 0.02$. This was in close agreement with the onset of microphase separation determined from the increase in the concentration of hydrogen-bonded urea carbonyls, previously obtained via infrared spectroscopy measurements.[4,5] However, the quantitative details of the correlation are hidden by the fact that each technique utilizes different information to detect the onset of microphase separation. The driving force for microphase separation is the thermodynamic incompatibility between the hard- and soft-segment blocks.[17] As polymerization proceeds, the degree of polymerization of the hard segment, N_H, increases. At a particular conversion of isocyanate, viz. $p_{NCO} = 0.54 \pm 0.02$, the number average hard-segment sequence length reaches a critical value; the product χN_H is such that the system is no longer thermodynamically stable [i.e. $\Delta G \geq 0$ and $(\partial^2 \Delta G/\partial \phi_H^2) \leq 0$]. The polym-

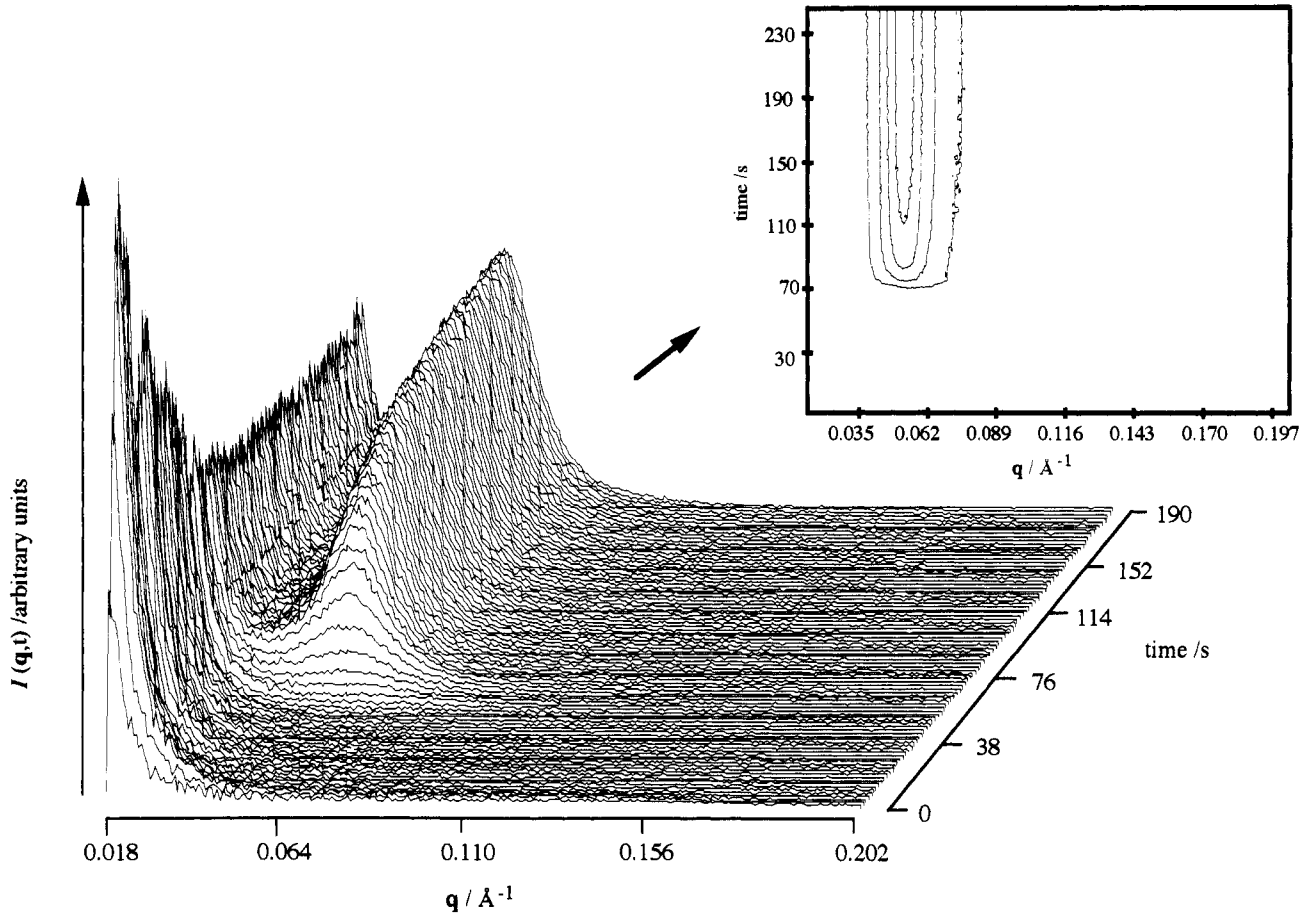

Figure 8. Three-dimensional plot of scattered intensity $I(q,t)$, versus scattering vector, q, versus reaction time, t, for a representative data set for the foaming system RIMSAXS-419. (b) Two-dimensional contour plot of time, t, versus scattering vector, q, for the 3-D data illustrated.

erization has acted as a large thermodynamic quench. The depth of this quench will determine the mechanism by which microphase separation occurs.

Interpretation of the Mechanism of Microphase Separation. The material that starts to form structure is a combination of homopolymer, block copolymers, and monomers and is discussed in terms of a mixture. The final structured material is predominantly a block copolymer, and thus the data are also analyzed in terms of the TDGL theory for microphase separation.[16] Depending upon the route a mixture follows through phase space, two very distinct mechanisms of phase separation are observed,[9,20,28,29] these being nucleation and growth and spinodal decomposition. Spinodal decomposition can lead to the formation of nonequilibrium morphologies comprising two interconnecting networks. On the other hand, nucleation and growth will lead to a continuous phase/dispersed phase morphology.[28,29] Both mechanisms have characteristic scattering signatures. The linearized theory of Cahn and Hilliard[20] predicts that the compositional fluctuations, and thus the scattered intensity, have a maximum for a given wavelength. In the early stages of the decomposition, there is an exponential increase in the scattered intensity with time. The nucleation and growth process is not well-defined in terms of a kinetic scattering theory. However, the scattered intensity should exhibit a monotonic decrease with an increase in scattering vector. It has been shown previously[30] that the scattered intensity at a fixed angle increases with the square of time for well-characterized nucleation and growth systems.

In order to critically investigate the mechanism of microphase separation, the evolution of structure was analyzed in several ways. Plots of $I(q,t)$ versus t^2 for both of the foaming systems indicated that there was no clear, distinct linear region. This was in stark contrast to the behavior observed previously of RIM polyurethane elastomers.[13] Further, an Avrami-type analysis of the form discussed for PU elastomers by Chu and co-workers[14,15] was attempted, but this resulted in very poor agreement between the predictions of both $I(q,t)$ and Q' as a function of time compared to that of the experimental data. The fact that a maximum in the scattering pattern was obtained, the failure of a linear dependence upon t^2 of the intensity at various scattering angles, and the poor fitting of an Avrami equation would seem to rule out nucleation and growth as the mechanism of microphase separation. If the mechanism of microphase separation is spinodal decomposition, the position of the maximum should remain constant but the peak intensity should exhibit an exponential increase with time. In the early stages of the decomposition, the microphase separating system is characterized by a high degree of interconnectivity between the phases. During the later stages of the decomposition, several ripening processes (Ostwald ripening[9]) can occur. This gives rise to an increase in the size of the interdomain spacing, and as a result q_{max} moves to smaller values.

In order to investigate if the mechanism of microphase separation was spinodal decomposition, the natural logarithm of the peak intensity, $I(q_{max},t)$, was plotted as a function of time. Parts a and b of Figure 12 show plots of the peak intensity, $I(q_{max},t)$, as a function of time for the foaming systems RIMSAXS-210 and RIMSAXS-419, respectively. It can be observed from both plots that there appears to be three distinct regions of phase behavior.

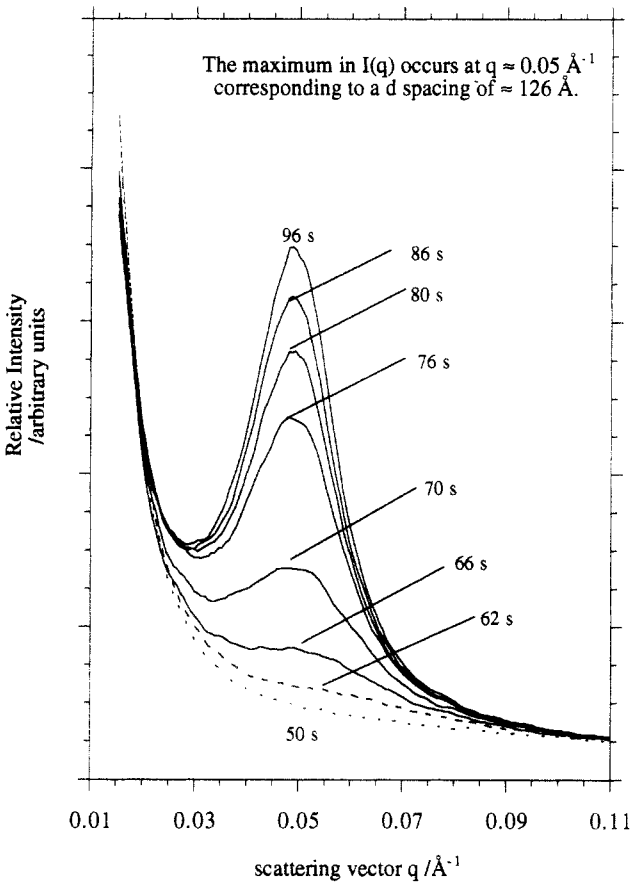

Figure 9. Plot of scattered intensity, $I(q)$, versus scattering vector, q, at selected times for a typical data set of the foaming system RIMSAXS-419.

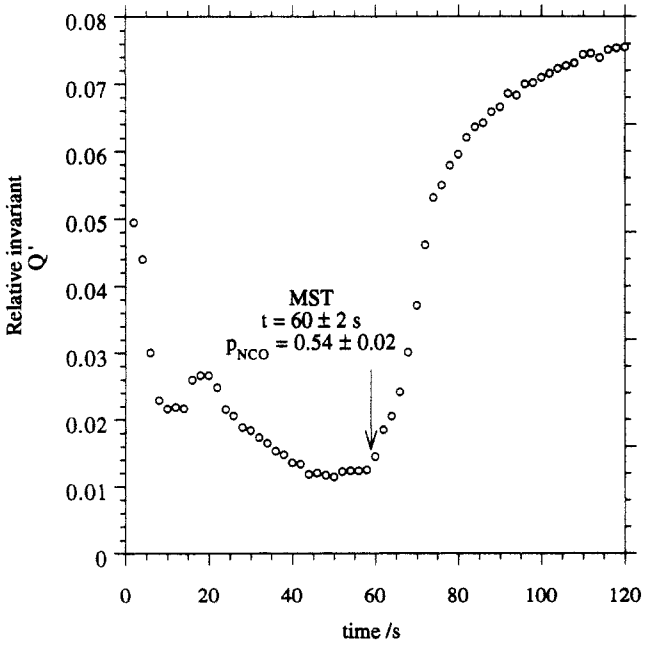

Figure 10. Plot of the relative invariant, Q', as a function of time, for a representative data set for the foaming system RIMSAXS-419.

Such behavior was reproducible on a run to run basis for both systems. The three regions previously described can be interpreted in the following way.

Region I. Initially, there is a homogeneous liquid mixture composed of unreacted monomer, homopolymer, urea hard-segment sequences, and isocyanate-tipped, polyether oligomers. At $p_{NCO} = 0.54 \pm 0.02$, the number average hard-segment sequence length, N_H, reaches a

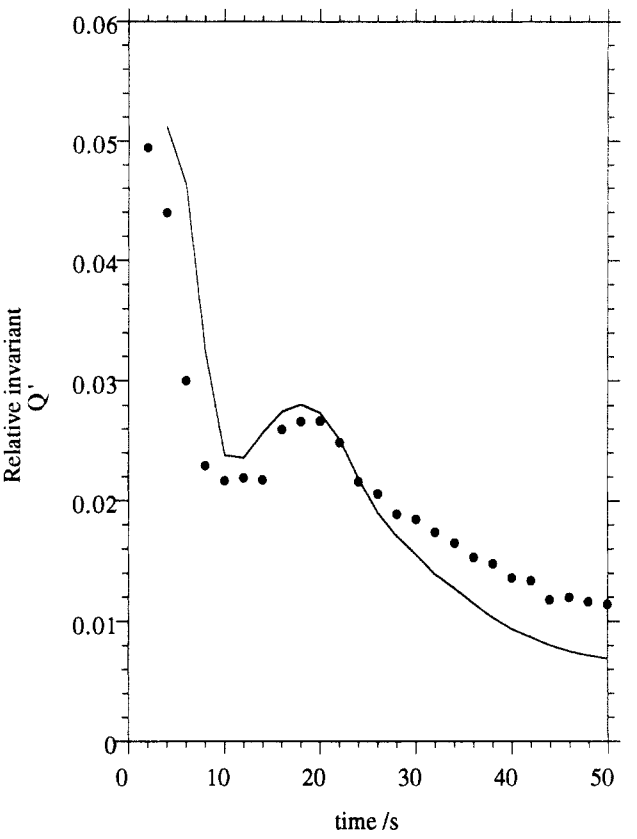

Figure 11. Comparison between the relative invariant predicted using eq 13 (solid line) and that observed from the experiment (●) from the same data set for the foaming system RIMSAXS-419 described in Figure 10.

critical value and the system becomes thermodynamically unstable.

Region II. This is the microphase separation transition (MST). Polymerization has provided the thermodynamic quench passing from the homogeneous (disordered), one-phase region of the phase diagram to the heterogeneous (ordered), two-phase region. The microphase-separated hard segments continue to grow, and association of these urea hard segments occurs. At the MST there is observed a rapid increase in the scattered intensity. It would appear that there is a good fit of the data to an exponential increase in intensity with time. This is in agreement with the linearized spinodal decomposition theory of Cahn and Hilliard.[20] The slope of the line provides a measure of the amplification rate, $(R(q))$ (eq 2), of the composition fluctuations. In the initial stages of the decomposition, the microphase-separating system should exhibit a high degree of interconnectivity between the phases.

Region III. In the case of RIMSAXS-210, after approximately 200 s the growth in the peak intensity slows down. Beyond 220 s, the peak intensity becomes approximately constant. This is after the expanding foam has reached the Berghmans point[26] (onset of vitrification, $p_{NCO} = 0.71 \pm 0.02$). In the case of RIMSAXS-419, at approximately 80 ± 2 s the growth in the peak intensity slows down and beyond 96 s the peak intensity becomes approximately constant. Again, this is after the expanding foam has reached the Berghmans point (onset of vitrification, $p_{NCO} = 0.71 \pm 0.02$). At this point, microphase separation is intercepted and quickly arrested by vitrification of the phase that is richer in hard segment. This phase has attained a composition with a T_g equal to that of the surrounding polymer medium. The intersection of the phase boundary and the T_g curve has been termed the

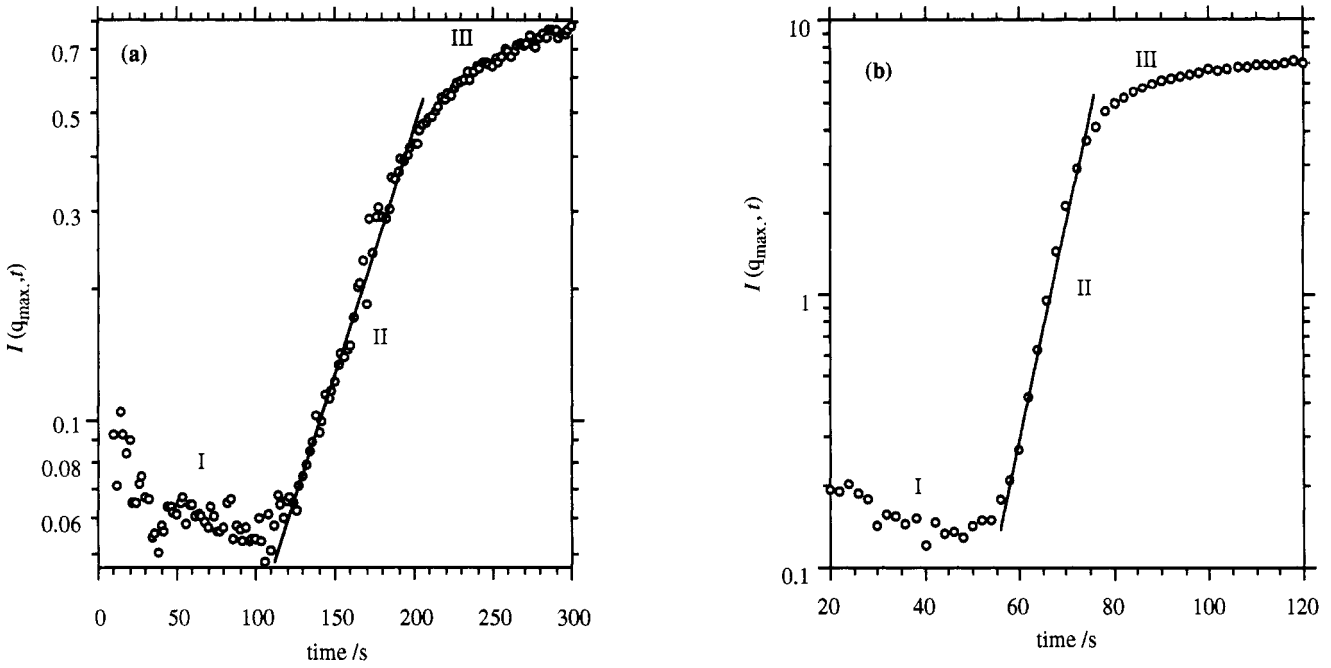

Figure 12. Plots of the density-corrected peak intensity, $I(q_{max},t)$, versus time, t, during foaming for (a) RIMSAXS-210 and (b) RIMSAXS-419. The symbols (O) are experimental data points and the solid line is a logarithmic fit (after Cahn and Hilliard[20]).

Berghmans point.[26] At or just prior to this point, the rate of association of urea hard segments passes through a maximum.[5] Almost immediately after this, cell opening is completed.

The vitrification of the hard segments freezes in the morphology at that time and results in the evolution of a foam with an internal polymer morphology that comprises an interconnecting physical network of domains of hydrogen-bonded urea hard-segment sequences within the cross-linked polyether–urethane. Rheological measurements[5] show an increase in the elastic shear modulus (G') of 2 orders of magnitude associated with vitrification, occurring at $p_{NCO} \approx 0.7$. In these systems, because microphase separation has been intercepted by glass transition, the ripening processes that can occur in the later stages of the decomposition cannot take place, and a shifting of q_{max} to lower values of scattering vector is not observed.

As originally published,[20] the Cahn–Hilliard theory gives a macroscopic description and has no direct relation to events at the molecular level. During polymerization, a number of block copolymer species are formed: first diblock and then multiblock, as the chain extension continues. Once the degree of polymerization reaches a critical value, microphase separation occurs. At the MST it has been previously shown[4,5] that there is a mixture of monomer, homopolymer, low molecular weight oligomers, and block copolymer present in these systems. The block copolymer theory proposed by Leibler[17] predicts that at the MST, an unstable mode with a nonvanishing wave vector appears in the system; i.e. a certain Fourier component of the monomer density fluctuations diverges. It is this instability that "triggers" the microphase separation transition. The wavelength of this Fourier component is set by the radius of gyration, R_g, of the longest block. In these systems it is the soft-segment polyether. The isocyanate tipped, polyether oligomers effectively act as a surfactant and stabilize the size scale of the subsequent phase growth. It has been shown that the structure which evolves has an interdomain spacing that is typical of polyether-based urethanes and is approximately 100–130 Å.[31-34]

Hashimoto and co-workers[11] have studied microphase separation in polystyrene–polyisoprene systems. Connell and co-workers[12] have also analyzed the kinetics of microphase separation in concentrated solutions of polystyrene–polyisoprene diblock copolymers during quenching experiments by time-resolved small angle neutron scattering (SANS). They both analyzed their data in terms of a time-dependent Ginzburg–Landau model (TDGL), and Connell and co-workers[12] observed that, for concentrated solutions of the block copolymer in cyclohexane (66% and 77% (w/w) block copolymer), plots of $R(q)/q^2$ versus q^2 exhibited a maximum at a finite value of scattering vector q. These observations were in qualitative agreement with the predictions of the TDGL theory. In the systems investigated in this study, if the mechanism of microphase separation is spinodal decomposition, then plots of $R(q)/"q^2$ versus q^2 should also exhibit a maximum at a finite value of q.

The values of $R(q)$ as a function of scattering vector were determined from plotting the natural logarithm of $I(q)$ versus time for values of q. The value of $R(q)$ is taken as half of the value of the slope of the line. Figure 13 is a plot of the natural logarithm of intensity, $I(q)$, versus time, t, for selected values of scattering vector, q. From such plots, values of $R(q)$ have been determined and then plotted in terms of $R(q)/q^2$ versus q^2. Figure 14 is a plot of $R(q)/q^2$ for representative data sets for the two foaming systems {RIMSAXS-210 lower curve, RIMSAXS-419 upper curve}.

From the curves it is apparent that both systems display the expected maximum at a finite value of the scattering vector. This is in qualitative agreement with the predictions of the TDGL theory. From the peak maxima in the curves, the optimum wavelength of spinodal decomposition, λ_s, and the effective diffusion coefficient, D_{eff}, of the polyether soft segment in the two foaming systems can be obtained. The value of λ_s determined for RIMSAXS-210 is 126 ± 3 Å and for RIMSAXS-419, 154 ± 2 Å. For the polyether soft segment, D_{eff} was calculated to be -4.9 ± 0.3 Å^2 s^{-1} in RIMSAXS-210 and -23.1 ± 0.6 Å^2 s^{-1} in RIMSAXS-419. Comparing the values with those ob-

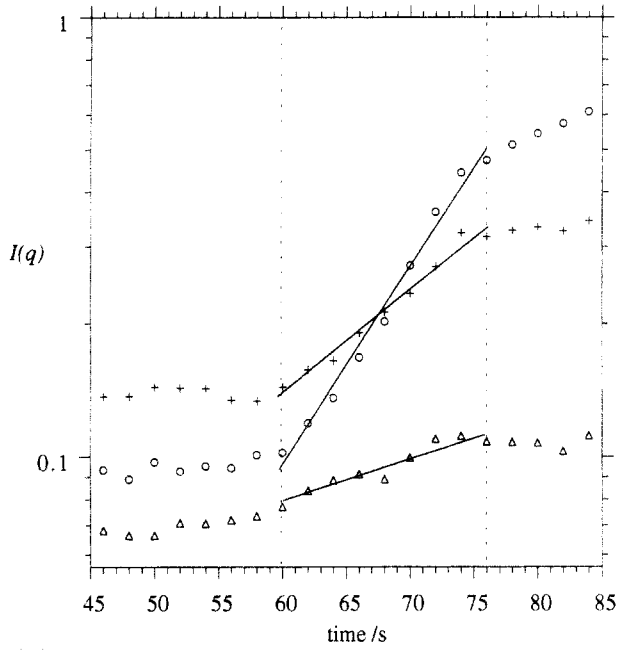

Figure 13. Plot of the density-corrected scattered intensity, $I(q)$, versus time, t, during foaming at scattering vector values of q = 0.036 (+), q = 0.050 (○), and q = 0.076 (▲).

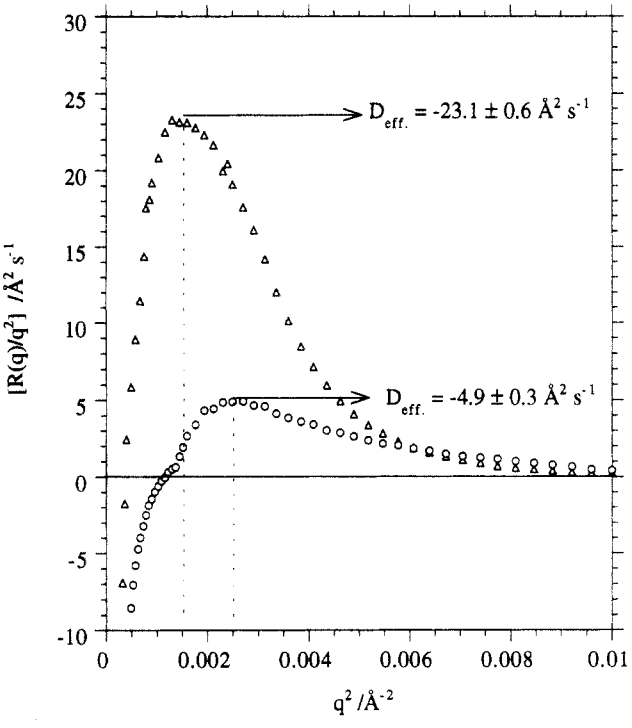

Figure 14. Plot of $R(q)/q^2$ versus q^2 for representative data sets obtained from the foaming systems RIMSAXS-210 (○) and RIMSAXS-419 (△).

tained by Connell and co-workers[12] for block copolymers with $\bar{M}_n$ of 8×10^4 (66% (w/w) block copolymer gave values of D_{eff} of -12.6 ± 0.8 to -20.5 ± 0.5 Å^2 s^{-1} for the quench temperature range 362–335 K and the 77% (w/w) block copolymer gave values of D_{eff} of -0.9 ± 0.6 up to -24.1 ± 0.5 Å^2 s^{-1} for the quench temperature range 369–323 K), the values are of the same order of magnitude. In addition, they observed that the effective diffusion coefficient increased with the increase in the depth of quench. This effect has also been observed for the current systems under investigation. However, it is important to point out that the value of $R(q)$ is strongly dependent upon χ_c and, thus, the value of D_{eff} obtained is also dependent upon χ_c.

By invoking the phase diagram of Leibler,[17] it is possible to estimate the value of $\chi_c(N_H + N_S)$. The values of N_H and N_S can be estimated by following the method of Ryan.[10,35] The volume fraction (ϕ_H) of hard segment is known and since the value of $\chi_c(N_H + N_S)$ can be estimated at a particular value of ϕ_H (abscissae) from the phase diagram of Leibler,[17] a value of χ_c can be obtained for each particular system. It is therefore possible to estimate the ratio $\chi_{c\text{-RIMSAXS-419}}/\chi_{c\text{-RIMSAXS-210}}$. This is effectively the ratio of the depths of quench of the two systems. It is found that the depth of quench for RIMSAXS-419 is approximately 1.7 times greater than that of RIMSAXS-210. It was observed that the wavelength of maximum growth rate, manifested as the d spacing (RIMSAXS-210, 105 Å, and RIMSAXS-419, 126 Å) is not coincident with that of the maximum thermodynamic driving force (RIMSAXS-210, 126 Å, and RIMSAXS-419, 154 Å).

It will be apparent that the difference between the two is approximately the same for both systems. The growth rate is dominated by R_g^2 ($\propto q_{max}^{-2}$), and the maximum will be very close to that of the experimentally observed maximum in the intensity as a function of q. However, $R(q)$ is obtained from simplified theory whereby the dependence of the free energy in terms of q of order greater than 2 are neglected. Inclusion of terms of higher order in q may shift the maximum in $R(q)/q^2$ to be coincident with the maximum in the growth rate in the scattering profiles.[12] Although the ratio of the depth of quench in the two systems cannot be quantitatively related to the ratio of diffusion coefficients, the important result that emerges from this analysis is that the microphase separation kinetics can be qualitatively described by a time-dependent Ginzburg–Landau model. This provides very strong evidence in favor of microphase separation proceeding via a spinodal decomposition type process during the foaming.

Summary and Conclusions

In this paper we have described how the technique of synchrotron small angle X-ray scattering can be applied to follow the kinetics of phase separation during the development of polymer morphology in the reactive processing of polyurethane foam. A forced-adiabatic SAXS reaction cell that can be positioned in the optical bench assembly of a beamline has also been described. Reproducible temperature control of the cell to within ±3 °C of the foam reaction exotherm over a period of 500 s has been observed across a range of foam exotherms and densities. The error in the isocyanate conversion obtained from the thermal response of the cell was ≤1% in the case of RIMSAXS-210 and ≤5% in the case of RIMSAXS-419. Close agreement was obtained between the free rise density calculated from the absorption of the X-rays and that measured from volume rise profiles by box foaming. The interdomain spacing for RIMSAXS-210 was found to be 105 Å and that for RIMSAXS-419, 126 Å. These were reproducible to within ±3 Å on a run to run basis. The interdomain spacings obtained were typical of polyether-based urethanes (≈100 Å). The onset of microphase separation was observed to occur at $p_{NCO} = 0.54 \pm 0.02$ for both foaming systems. This was in close agreement with the onset of microphase separation detected by FT-IR spectroscopy. For both systems, a plot of the natural logarithm of the peak intensity, $I(q_{max},t)$, as a function of time exhibited three distinct regions of behavior associated with reaction in the homogeneous phase, microphase separation, and vitrification. The analysis of the scattering data in terms of a time-dependent Ginzburg–Landau

model (TDGL) yielded results that were in qualitative agreement with the predictions of the TDGL theory. The values of the effective diffusion coefficients, D_{eff}, of the polyether soft segment were found to be -4.9 ± 0.3 Å^2 s^{-1} for RIMSAXS-210 and -23.1 ± 0.6 Å^2 s^{-1} for RIMSAXS-419. The most important result that emerged from the SAXS experiments was that the microphase separation kinetics could be qualitatively described by a time-dependent Ginzburg–Landau model. From this it is concluded that microphase separation of urea hard segments during the formation of flexible polyurethane foam proceeds via a spinodal decomposition type of process.

Acknowledgment. We would like to thank Dow Benelux N.V., Terneuzen, The Netherlands, for suggesting this problem and providing the necessary financial support. The SERC provided beamtime at the Daresbury SRS under Minor Grant 21/109. Finally, it is a pleasure to acknowledge the technical support of Dr. Wim Bras, without whom the experiments would not have been possible.

References and Notes

(1) Artavia, L. D.; Macosko, C. W. *Proc. SPI Annu. Tech./Mark. Conf., 33rd* **1990**, 554.
(2) Priester, R. D., Jr.; McClusky, J. V.; O'Neill, R. E.; Turner, R. B.; Harthcock, M. A.; Davis, B. L. *Proc. SPI Annu. Tech./Mark. Conf., 33rd* **1990**, 527.
(3) Artavia, L. D. Ph.D. Thesis, University of Minnesota, 1991.
(4) Elwell, M. J. A.; Ryan, A. J.; Grünbauer, H. J. M.; Van Lieshout, H. C.; Thoen, J. A. *Prog. Rubber Plast. Technol.* **1993**, *9*, 120.
(5) Elwell, M. J. A. Ph.D. Thesis, Victoria University of Manchester, 1993.
(6) Turner, R. B.; Spell, H. L.; Wilkes, G. L. *Proc. 28th SPI Annu. Tech./Mark. Conf., 28th* **1988**, 244.
(7) Armistead, J. P.; Turner, R. B.; Wilkes, G. L. *J. Appl. Polym. Sci.* **1988**, *35*, 601.
(8) Creswick, M. W.; Lee, K. D.; Turner, R. B.; Huber, L. M. *Proc. SPI Annu. Tech./Mark. Conf., 31st* **1988**, 11.
(9) Ryan, A. J. *Polymer* **1990**, *31*, 707.
(10) Ryan, A. J.; Stanford, J. L.; Still, R. H. *Plast. Rubber Process. Appl.* **1990**, *13*, 99.
(11) Hashimoto, T.; Kowsaka, K.; Shibayama, M.; Kawai, H. *Macromolecules* **1986**, *19*, 754.
(12) Connell, J. G.; Richards, R. W.; Rennie, A. R. *Polymer* **1991**, *32*, 2033.
(13) Ryan, A. J.; Willkomm, W. R.; Bergstrom, T. B.; Macosko, C. W.; Koberstein, J. T.; Yu, C. C.; Russell, T. P. *Macromolecules* **1991**, *24*, 2883.
(14) Li, Y.; Gao, T.; Chu, B. *Macromolecules* **1992**, *25*, 1737.
(15) Chu, B.; Gao, T.; Li, Y.; Wang, J.; Desper, C. R.; Byrne, C. A. *Macromolecules* **1992**, *25*, 5724.
(16) Hashimoto, T. *Macromolecules* **1987**, *20*, 465.
(17) Leibler, L. *Macromolecules* **1980**, *13*, 1602.
(18) Cook, H. E. *Acta Metall.* **1970**, *18*, 297.
(19) Pincus, P. *J. Chem. Phys.* **1981**, *75*, 1996.
(20) Cahn, J. W.; Hilliard, J. *J. Chem. Phys.* **1958**, *28*, 258.
(21) de Gennes, P. G. *J. Chem. Phys.* **1980**, *72*, 4756.
(22) Binder, K. *Colloid Polym. Sci.* **1987**, *265*, 373.
(23) Mikkleson, K.; Macosko, C. W. *J. Cell. Plast.* **1989**, *21*, 29.
(24) Yang, W. P.; Macosko, C. W. *Die Makromol. Chem., Macromol. Symp.* **1989**, *25*, 23.
(25) Kanner, B.; Decker, T. G. *J. Cell. Plast.* **1969**, *5*, 32.
(26) Callister, S.; Keller, A.; Hikmet, R. M. *Makromol. Chem. Makromol. Symp.* **1990**, *39*, 19.
(27) Ryan, A. J.; Macosko, C. W.; Bras, W. *Macromolecules* **1992**, *25*, 6277.
(28) Olabisi, O.; Robeson, L. M.; Shaw, M. T. *Polymer-Polymer Miscibility*; Academic Press: New York, 1977.
(29) Binder, K. In *Phase Transformations in Materials*; Cahn, R. W., Haasen, P., Kramer, E. J., Eds.; Materials Science and Technology: A Comprehensive Treatment; VCH Publishers: Weiheim, 1991; Chapter 7, p 405.
(30) Lipatov, Y. S.; Grigor'yeva, O. P.; Kovernick, G. P.; Shilov, V. V.; Sergryeva, L. M. *Makromol. Chem.* **1985**, *186*, 1401.
(31) Koberstein, J. T.; Russell, T. P. *Macromolecules* **1986**, *19*, 714.
(32) Koberstein, J. T.; Stein, R. S. *J. Appl. Polym. Sci., Poly. Phys. Ed.* **1983**, *21*, 1439.
(33) Leung, L. M.; Koberstein, J. T. *Macromolecules* **1986**, *19*, 706.
(34) Galambos, A. F. Ph.D. Thesis, University of Princeton, 1989.
(35) Ryan, A. J. Ph.D. Thesis, Victoria University of Manchester, 1988.